SCALE EFFECTS IN MEDIA WITH PERIODIC AND NEARLY PERIODIC MICROSTRUCTURES — II. FAILURE MECHANISMS

by:

M. SCHRAAD and N. TRIANTAFYLLIDIS

Published in the: Journal of Applied Mechanics, 1997, Volume 64, pp.762-771

SCALE EFFECTS IN MEDIA WITH PERIODIC AND NEARLY PERIODIC MICROSTRUCTURES — II. FAILURE MECHANISMS

by:

M. SCHRAAD and N. TRIANTAFYLLIDIS

Department of Aerospace Engineering

The University of Michigan

Ann Arbor, Michigan 48109-2118

Abstract

Using the nonlinearly elastic, planar, lattice model presented in Part I, the influence of scale (i.e., the size of the representative volume, relative to the size of the unit cell) on the onset of failure in periodic and nearly periodic media is investigated. For this study, the concept of a micro-failure surface is introduced — this surface being defined as the locus of first instability points found along radial load paths through macroscopic strain space. The influence of specimen size and microstructural imperfections (both geometric and constitutive) on these failure surfaces is investigated. The micro-failure surface determined for the infinite model with perfectly periodic microstructure, is found to be a lower bound for the failure surfaces of perfectly periodic, finite models, and an upper bound for the failure surfaces of finite models with microstructural imperfections. The concept of a macro-failure surface is also introduced — this surface being defined as the locus of points corresponding to the loss of ellipticity in the macroscopic (homogenized) moduli of the model. The macro-failure surface is easier to construct than the micro-failure surface, because it only requires calculation of the macroscopic properties for the unit cell, at each loading state along the principal equilibrium path. The relation between these two failure surfaces is explored in detail, with attention focused on their regions of coincidence, which are of particular interest due to the possible development of macroscopically localized failure modes.

1 INTRODUCTION

The influence of scale on the macroscopic properties of microstructured media was the subject of Part I of this investigation. Of primary interest in Part II, is the influence of scale on the onset of failure in these materials. Defining failure in composite and microstructured media can be a relatively daunting and intricate task. The complexity involved, stems from the multitude of simultaneously occurring failure mechanisms, some of which are present, even at negligible levels of loading. In the present investigation, attention is restricted to ductile solids with periodic and nearly periodic microstructures, since in addition to the existence of a well defined geometric scale parameter ϵ (which characterizes the size of representative volume, relative to the size of the unit cell), one can also define the onset of failure as the first buckling-type instability encountered along a load path which begins from the undeformed, stress-free state.

In addition to the influence of the geometric and imperfection scales introduced in Part I, the onset of failure investigation involved in Part II explores the influence of a new scale, characterized by the parameter ω_c, which is associated with the resulting instability mode (ω_c is defined as the ratio of the unit cell size, to the wavelength of first bifurcation mode shape at criticality). This critical mode shape scale establishes whether the onset of failure is a global ($\omega_c \to 0$) or local ($\omega_c \neq 0$) phenomenon. With regard to the different length scales involved, there are three fundamental questions which need to be addressed for this general class of rate-independent, periodic, ductile solids, when subjected to general, macroscopic, finite strain loadings. First, what is the critical mode shape scale parameter ω_c associated with such a medium, for a given macroscopic loading, in the absence of boundary effects? Second, under what conditions can the failure of these materials be predicted from the macroscopic properties found in Part I? And third, what is the influence of the geometric scale, the imperfection shape, and the imperfection amplitude, on the critical load and bifurcation mode shape, at the onset of failure?

The present work is closely related to earlier research, conducted by one of the authors, on the stability of finitely strained, periodic composites. The issues concerning the critical mode shape scale parameter were first investigated using exact calculations involving ω_c, for the case of axially deformed, layered composites under plane strain conditions, by Triantafyllidis and Maker (1985). Subsequent work by Geymonet, Müller and Triantafyllidis (1993), illustrated the completeness of the Bloch wave representation for capturing the first instability in finitely strained, perfectly periodic composites in three dimensions, and proved that in the case for which $\omega_c \to 0$, the first instability can also be determined from the macroscopic properties of the infinite medium, as the first loss of ellipticity in the homogenized moduli of the material. Lastly, the concepts of micro- and macro-failure surfaces for finitely strained, periodic media were introduced by Triantafyllidis and Schnaidt (1993), for the case of biaxially stressed truss

models. All of this work, however, concerns perfectly periodic media of infinite extent. The influence of the geometric scale, and the effects of microstructural imperfections on the onset of failure in these materials were not previously addressed (since the corresponding calculations are orders of magnitude more complicated). These topics, therefore, are the subject of the present investigation.

It should be mentioned at this point that the stability of periodic, lattice-type structures, and the use of continuum models for the investigation of their behavior, is not a novel idea. The investigation of the stability for both the resulting continuum (macroscopic) models, as well as for the exact (microscopic) models, has been the subject of a number of previous investigations (see, for example, Forman and Hutchinson, 1970, for an investigation involving reticulated shell structures, and Elyada and Babcock, 1987, for a similar study of truss columns, etc.). The traditional approach to these problems, thus far, has involved the study of the exact (microscopic) model of a particular material or structure, when subjected to specific loading conditions (see, for example, Anderson, 1981, for a general formulation of the stability problem for periodic truss structures). In cases when a continuum model has also been used, no systematic investigation of the validity of the nonlinear continuum (macroscopic) model, under all possible macroscopic strains, has been presented. Furthermore, an investigation of scale effects in such problems, which requires the comparison of solutions to boundary value problems with fixed macroscopic dimensions and loading, but with a variety of unit cell sizes, has not been undertaken, thus far, to the best of the authors' knowledge. Moreover, although some work has already been devoted to the subject of imperfection sensitivity in the exact models (see, for example, Anderson, 1986), a systematic investigation of the influence of geometric and constitutive microstructural imperfections on the first buckling-type instability in this class of materials remains to be initiated. Finally, on the experimental side, the only consistent investigation of scale effects on the failure of periodic composites, known to the authors, was undertaken by Greszuck (1975), who tested a series of self-similar, fiber-reinforced composites under axial compression.

The method used to address the previously posed questions concerning the geometric and imperfection scale dependence of the failure mechanisms of ductile media with periodic microstructures under finite strains, involves the nonlinear, periodic, lattice model introduced in Part I. For this idealized model, a microscopic failure surface, which corresponds to the onset of the first local instability mode, and a macroscopic failure surface, which corresponds to the first loss of ellipticity in the macroscopic (homogenized) behavior of the model, are defined in macroscopic strain space. In view of the relative simplicity of the lattice model, detailed investigations are conducted to find the critical mode shape scale parameter ω_c, and to determine the influence of the geometric and imperfection scales on the shape of the corresponding failure surfaces, for all possible states of macroscopic strain. The relation between the micro- and

macro-failure surfaces is explored further, with attention focused on their regions of coincidence, which are of particular interest due to the possibility of macroscopically localized instability modes developing at the onset of failure.

A sequence of calculations is proposed which allows the construction of the failure surfaces for the perfectly periodic medium. The methodology proceeds from the simplest calculations involved in the construction of the macro-failure surface for the perfectly periodic, infinite model, to the more complex calculations used to construct the micro-failure surface. This methodology also illustrates how to bound the actual failure surface of a real (imperfect), microstructured medium, for which the onset of failure calculations in an actual application would be prohibitively time consuming. The proposed methodology is applicable to periodic media, with both discrete and continuum microstructures.

2 FAILURE MECHANISMS

The ultimate failure of ductile solids with periodic microstructures can be related to the onset of a buckling-type instability. Consequently, for the idealized lattice models considered here, failure is defined as the loss of stability in the material behavior. Of particular interest is the first instance of instability, which for the nonlinearly elastic model, coincides with the first loss of positive definiteness in the incremental stiffness matrix of the model. For a perfectly periodic lattice model, the onset of the first instability corresponds to a bifurcation in the principal equilibrium solution (i.e., the solution for which all unit cells deform identically), while for a lattice model with microstructural imperfections, the first instability corresponds to a maximum load.

The representative volume of the perfectly periodic model, which is comprised of $N \times N$ unit cells (see Figure 1a of Part I), is subjected to a macroscopic strain characterized by the deformation gradient tensor $\mathbf{F}_0(\lambda)$ defined in equations (6) – (8) of Part I. This macroscopic loading is imposed by prescribing the boundary displacements to the representative volume (Dirichlet boundary conditions) for the case of finite sized specimens.

The loading of the lattice models follows radial paths through macroscopic strain space. Each load path is parameterized by the scalar load parameter λ, and corresponds to a macroscopic deformation gradient tensor $\mathbf{F}_0(\lambda)$, with a fixed principal macroscopic strain orientation angle θ, and a fixed ratio of principal macroscopic stretch ratios characterized by a constant load path angle ϕ (see the definitions in equations (6) and (7) of Part I). As the load parameter increases from zero ($\lambda = 0$ corresponds to the stable, undeformed, stress-free configuration) the principal equilibrium solution remains stable until a critical value, denoted by λ_c and termed the "*critical load*", is reached, at which the model first loses stability. A micro-failure surface for the representative volume can thus be defined in macroscopic strain space. This failure surface corresponds to the locus of all critical principal stretch ratios $(\lambda_1(\lambda_c), \lambda_2(\lambda_c))$, which are calculated for a fixed principal strain orientation angle θ.

Of interest in the present work is the influence of scale and the effects of imperfections on the previously defined failure surfaces. For a finite sized lattice model, comprised of $N \times N$ unit cells, the relevant scale is characterized by the geometric scale parameter $\epsilon = h/H = 1/N$, defined in Part I. For an infinite specimen (i.e., for $\epsilon \to 0$) with perfectly periodic microstructure, a different scale parameter becomes relevant — namely, the bifurcation mode shape scale parameter ω, which is defined as the ratio of the unit cell size, to the wavelength of the bifurcation eigenmode. In the remainder of this section, the theoretical aspects of the onset of failure calculations are developed, initially for the infinite lattice model with perfectly periodic microstructure, and then for the finite lattice models.

2.1 INFINITE PERIODIC MODEL — MICRO-FAILURE SURFACE

Consider first the construction of the micro-failure surface for the infinite lattice model with perfectly periodic microstructure. The corresponding calculations are considerably less involved than those required to construct the corresponding failure surface for the finite model, because they are based on the incremental response of the unit cell along the principal equilibrium solution. Although the corresponding methodology, which is based on Bloch wave theory, has been presented in Triantafyllidis and Schnaidt (1993) for the case of discrete models, and by Triantafyllidis and Bardenhagen (1997) for continuum models, the calculations are briefly outlined here, for reasons of completeness.

By definition, for each load path defined by the macroscopic deformation gradient tensor $\mathbf{F}_0(\lambda)$, the critical load parameter λ_c corresponds to the first instance of instability in the infinite model, which also coincides with the first singular point in the incremental stiffness matrix of the system. As a result, the incremental equilibrium of the model, at the critical principal state, admits a non-trivial solution in the absence of externally imposed loading. The relationship between the increments in the nodal force vectors $\dot{\mathbf{f}}_p$, exerted by all elements of node p that do not belong to the unit cell, and the corresponding displacement increment vectors $\dot{\mathbf{u}}_q$, at node q of the unit cell (see the insert of Figure 1a), is

$$\dot{\mathbf{f}}_p = \mathbf{K}_{pq} \cdot \dot{\mathbf{u}}_q, \qquad 1 \leq p, q \leq 4, \tag{1}$$

where

$$\mathbf{K}_{pq} = \begin{bmatrix} K_{2p-1,2q-1} & K_{2p-1,2q} \\ K_{2p,2q-1} & K_{2p,2q} \end{bmatrix} \qquad \text{and} \qquad K_{ij} = \frac{\partial^2 \mathcal{E}_{cell}}{\partial u_i \partial u_j}. \tag{2}$$

Recall from Part I, that $\mathcal{E}_{cell}$ is the total strain energy of the unit cell, and u_i are the corresponding eight displacement degrees of freedom ($\mathbf{u}_p = (u_{2p-1}, u_{2p})$, where u_{2p-1} and u_{2p} are the X_1 and X_2 displacements, respectively, of node p). The derivative of the strain energy $\mathcal{E}$ is evaluated at the stressed state defined by $\mathbf{F}_0(\lambda)$, and consequently, all components of the stiffness matrix $\mathbf{K}_{pq}$ of the unit cell are functions of the macroscopic deformation gradient tensor $\mathbf{F}_0(\lambda)$.

It can be shown (see, for example, Lomont, 1959, for analysis pertaining to the stability of lattice systems) that at the critical load defined by λ_c, the displacement increment vector $\dot{\mathbf{u}}\,(X_1, X_2)$ can always assume the following form:

$$\dot{\mathbf{u}}\,(X_1, X_2) = \exp[i(\omega_1 X_1 + \omega_2 X_2)/h]\mathbf{p}(X_1, X_2), \tag{3}$$

where $i = \sqrt{-1}$, ω_1/h and ω_2/h are the wave numbers of the corresponding bifurcation eigenmode along the X_1 and X_2 directions, respectively, and $\mathbf{p}(X_1, X_2)$ is a periodic function of X_1 and X_2, with the same spatial periodicity as the unit cell (i.e., $\mathbf{p}(X_1 + n_1 h, X_2 + n_2 h) = \mathbf{p}(X_1, X_2)$, where n_1 and n_2 are arbitrary integers).

The representation of $\dot{\mathbf{u}}$ given in equation (3) implies the following relationships between the nodal force and displacement increment vectors of the unit cell:

$$\dot{\mathbf{u}}_2 = \mu_1 \, \dot{\mathbf{u}}_1, \qquad \dot{\mathbf{u}}_3 = \mu_1 \mu_2 \, \dot{\mathbf{u}}_1, \qquad \dot{\mathbf{u}}_4 = \mu_2 \, \dot{\mathbf{u}}_1; \tag{4}$$

and

$$\dot{\mathbf{f}}_2 = -\mu_1 \, \dot{\mathbf{f}}_1, \qquad \dot{\mathbf{f}}_3 = \mu_1 \mu_2 \, \dot{\mathbf{f}}_1, \qquad \dot{\mathbf{f}}_4 = -\mu_2 \, \dot{\mathbf{f}}_1; \tag{5}$$

where

$$\mu_1 = \exp(i\omega_1), \qquad \text{and} \qquad \mu_2 = \exp(i\omega_2). \tag{6}$$

Introducing relations (4) and (5) into the incremental force-displacement relation (1), the following equivalent system can be obtained solely in terms of $\dot{\mathbf{u}}_1$:

$$\widehat{\mathbf{K}}(\lambda, \boldsymbol{\omega}) \cdot \dot{\mathbf{u}}_1 = \mathbf{0}, \qquad \text{where} \qquad \boldsymbol{\omega} = (\omega_1, \omega_2), \tag{7}$$

and where $\widehat{\mathbf{K}}$ is a reduced, 2×2, Hermitian matrix (i.e., $\widehat{\mathbf{K}}^T = \overline{\widehat{\mathbf{K}}}$, where $\overline{\widehat{\mathbf{K}}}$ is the complex conjugate of $\widehat{\mathbf{K}}$). The matrix $\widehat{\mathbf{K}}$ is the stability matrix of the infinite model with perfectly periodic microstructure, which is strained by $\mathbf{F}_0(\lambda)$, and subjected to the quasi-periodic condition defined in equation (3). Let $\lambda_m(\boldsymbol{\omega})$ denote the minimum root of the equation $\det(\widehat{\mathbf{K}}(\lambda, \boldsymbol{\omega})) = 0$, for a fixed dimensionless wave number vector $\boldsymbol{\omega}$, that is,

$$\lambda_m(\boldsymbol{\omega}) = \text{min root of} \left\{ \det[\widehat{\mathbf{K}}(\lambda, \boldsymbol{\omega})] = 0 \right\}. \tag{8}$$

Thus, $\lambda_m(\boldsymbol{\omega})$ defines a critical load parameter surface in dimensionless wave number space, and therefore, the critical load parameter λ_c is defined as the minimum value of $\lambda_m(\boldsymbol{\omega})$ over all dimensionless wave number vectors $\boldsymbol{\omega}$ (i.e., for $0 \leq \omega_1, \omega_2 \leq 2\pi$):

$$\lambda_c = \min_{0 \leq \omega_1, \omega_2 \leq 2\pi} \lambda_m(\boldsymbol{\omega}) = \lambda_m(\boldsymbol{\omega}_c). \tag{9}$$

There are two important characteristics of the critical load parameter surface $\lambda_m(\boldsymbol{\omega})$ which require discussion at this point. The first has to do with the symmetries of this surface in the dimensionless wave number domain. Notice that for situations involving pure biaxial deformation (i.e., for load paths with $\theta = 0$), the principal equilibrium solution is symmetric with respect to both the X_1 and X_2 coordinate axes, as well as point-symmetric about the center of the unit cell. These symmetries imply the following relationships for the stability matrix $\widehat{\mathbf{K}}(\lambda, \boldsymbol{\omega})$, defined in equation (7), for $\theta = 0$:

$$\widehat{\mathbf{K}}(\lambda, \omega_1, \omega_2) = \widehat{\mathbf{K}}(\lambda, 2\pi - \omega_1, \omega_2) = \widehat{\mathbf{K}}(\lambda, \omega_1, 2\pi - \omega_2) = \widehat{\mathbf{K}}(\lambda, 2\pi - \omega_1, 2\pi - \omega_2). \tag{10}$$

The same symmetry relations that hold for the stability matrix $\widehat{\mathbf{K}}(\lambda, \boldsymbol{\omega})$ also hold for the critical load parameter surface, and hence, $\lambda_m(\boldsymbol{\omega})$ is only calculated for the domain $0 \leq \omega_1, \omega_2 \leq \pi$.

For instances when the principal strain axes are oriented at an angle $\theta \neq 0$ with respect to the initial axes of material orthotropy, the principal equilibrium solution is only point-symmetric about the center of the unit cell. This symmetry implies the following relationship for the stability matrix $\widehat{\mathbf{K}}(\lambda, \boldsymbol{\omega})$ for $\theta \neq 0$:

$$\widehat{\mathbf{K}}(\lambda, \omega_1, \omega_2) = \widehat{\mathbf{K}}(\lambda, 2\pi - \omega_1, 2\pi - \omega_2). \tag{11}$$

Again, the same symmetry relationship should also hold for the critical load parameter surface, and thus $\lambda_m(\boldsymbol{\omega})$ is only calculated in the domain $0 \leq \omega_1 + \omega_2 \leq 2\pi$.

The second important characteristic of the critical load parameter surface $\lambda_m(\boldsymbol{\omega})$ concerns the presence of a singularity at the origin of the dimensionless wave number domain (i.e., at $\boldsymbol{\omega} = (0, 0)$). Notice that two different types of bifurcation eigenmodes are mapped in the neighborhood of the origin: the periodic modes (since the eigenmode corresponding to $\omega_1 = \omega_2 = 0$ has wavelengths in each direction which are commensurate with the corresponding unit cell size), and the long wavelength modes, (i.e., the modes with wavelengths $L_i \gg h$, since the corresponding dimensionless wave numbers $(\omega_1, \omega_2) = (2\pi h/L_1, 2\pi h/L_2) \rightarrow (0, 0)$). The critical load for a long wavelength mode does not, in general, coincide with the critical load of a periodic mode, and hence, the critical load parameter surface $\lambda_m(\boldsymbol{\omega})$ is singular at the origin (see Figure 3).

Since the geometric scale parameter is identically zero for the infinite model (i.e., $\epsilon \rightarrow 0$), the relevant scale parameter is ω, which is defined as the magnitude of the dimensionless wave number vector,

$$\omega = \|\boldsymbol{\omega}\| = \left[(\omega_1)^2 + (\omega_2)^2 \right]^{1/2}, \tag{12}$$

and is termed the "*mode shape scale*" parameter.

Two different situations are distinguished, according to whether or not the corresponding critical mode shape scale parameter ω_c is zero at the critical load λ_c. For $\omega_c \neq 0$, the onset of failure is termed "*local*", because the critical eigenmode has a wavelength commensurate with the unit cell size. For $\omega_c \to 0$ (i.e., when the critical load parameter surface has a singularity at the origin, and hence, $\lambda_m(0,0)$ cannot be defined — which is always the case for the lattice model under investigation), the onset of failure is termed "*global*", because the critical eigenmode has a wavelength which is much larger than the unit cell size. For the latter case, the failure mode depends on the overall properties of the lattice at the loading state in question, and therefore, the critical load for this case can be found with considerably less effort by investigating the macroscopic (homogenized) properties of the model. Consequently, one can extend this approach, and construct a new failure surface for the model, which is based on the macroscopic properties. The resulting failure surface, which is a more easily obtainable upper bound for the computationally intensive, exact or "*micro-failure*" surface, is termed the "*macro-failure*" surface, and is defined immediately below.

2.2 INFINITE PERIODIC MODEL — MACRO-FAILURE SURFACE

The macro-failure surface, determined for the infinite lattice model, is defined in macroscopic strain space using the loss of ellipticity of the macroscopic (homogenized) moduli tensor $\mathbf{L}(\lambda)$, defined in equation (15) of Part I, as the onset of failure criterion. More specifically, the macroscopic critical load, denoted by λ_e, is defined as the minimum value of the load parameter λ, along a given load path (i.e., for fixed ϕ and θ), for which the rank two tensor $\mathbf{n}\cdot\mathbf{L}(\lambda)\cdot\mathbf{n}$ (termed the "*acoustic tensor*") loses positive definiteness, that is,

$$\lambda_e = \text{min root of} \{ d(\lambda) = 0 \}, \tag{13}$$

where

$$d(\lambda) = \min_{\|\mathbf{n}\|=1} \det \left(L_{ijkl}(\lambda)\, n_j n_l \right). \tag{14}$$

As shown by Triantafyllidis and Schnaidt (1993) for materials with discrete, periodic microstructures, and by Geymonet, Müller and Triantafyllidis (1993) for general periodic continua, the macroscopic critical

load is always greater than or equal to the microscopic critical load (i.e., $\lambda_e \geq \lambda_c$), with the equality achieved when $\omega_c \to 0$. Hence, the macro-failure surface for an infinite lattice model with perfectly periodic microstructure provides an upper bound for the corresponding micro-failure surface.

Notice that the construction of the macro-failure surface is based on a simple algebraic manipulation of the macroscopic (homogenized) incremental moduli tensor $\mathbf{L}(\lambda)$, which is calculated only once at each increment along the load path of interest. Alternatively, the construction of the micro-failure surface requires, at each increment, the calculation of the reduced stiffness matrix $\widehat{\mathbf{K}}(\lambda, \boldsymbol{\omega})$, for a sufficient number of dimensionless wave number vectors $\boldsymbol{\omega}$ (to adequately cover the dimensionless wave number domain, and accurately predict the critical load and bifurcation mode shape). Consequently, the calculation of the macro-failure surface is considerably less intensive computationally than the calculation of the corresponding micro-failure surface. In general, the ratio of the two calculation times is roughly equal to the number of grid points used to cover the dimensionless wave number domain, which for the calculations reported here is of the order of 10^3 to 10^4.

The locus of points in macroscopic strain space for which the micro- and macro-failure surfaces coincide (i.e., the points for which $\omega_c \to 0$), is of particular interest here for two reasons. First, it determines a range of validity for the failure predictions obtained from the macroscopic properties determined by homogenization theory, since for the macroscopic strains in question, a local instability does not precede an instability which is global in nature. And second, for the critical load states for which the first instability in the infinite medium with perfectly periodic microstructure is global in nature, the post-bifurcation failure mode is likely to develop into a macroscopically localized mode of failure (of the shear band or kink band type). As discussed in detail in Triantafyllidis and Bardenhagen (1997), the determination of the range of deformations, defined by $\mathbf{F}_0(\lambda)$, for which the micro- and macro-failure surfaces do not coincide, is based on calculations involving the higher order gradient homogenized moduli tensor $\mathbf{B}$, introduced in equation (23) of Part I.

According to Triantafyllidis and Bardenhagen (1997), a sufficient condition, which ensures that the micro- and macro-failure surfaces do not coincide, is based on the sign of the *failure surface separation parameter* β. This scalar parameter is the minimum eigenvalue of the stiffness matrix, for a model subjected to a rank one macroscopic deformation gradient (i.e., subjected to $\mathbf{F} = \boldsymbol{\alpha} \otimes \mathbf{n}$), and is defined by

$$\beta = B_{ijklmn}\left(\lambda_e\right) \alpha_i^e n_j^e n_k^e \alpha_l^e n_m^e n_n^e, \tag{15}$$

where the vectors $\mathbf{n}^e$ and $\boldsymbol{\alpha}^e$ are determined from the following conditions, respectively:

$$\det\left(L_{ijkl}\left(\lambda_e\right) n_j^e n_l^e\right) = 0, \qquad L_{ijkl}\left(\lambda_e\right) n_j^e \alpha_k^e n_l^e = 0. \tag{16}$$

Here, $\mathbf{n}^e$ is the unit vector for which the acoustic tensor $\mathbf{n}\cdot\mathbf{L}(\lambda)\cdot\mathbf{n}$ first loses positive definiteness, and $\boldsymbol{\alpha}^e$ is the corresponding eigenvector of the acoustic tensor at the macroscopic critical load λ_e. When the failure surface separation parameter β is less than zero, it can be shown that the first instability in the perfectly periodic lattice is local in nature, and therefore, the micro- and macro-failure surfaces do not coincide. The proposed sufficient condition is based on the macroscopic properties of the model, and provides the means to determine, in a computationally efficient manner, the region of the macro-failure surface which cannot be reached due to the occurrence of a prior, local instability.

2.3 FAILURE SURFACES FOR FINITE MODELS

Following the determination of the micro- and macro-failure surfaces for the infinite lattice model with perfectly periodic microstructure — which are based on calculations involving only the unit cell — attention is focused on the failure surfaces for finite size specimens comprised of $N\times N$ unit cells. Of interest here is the influence of the geometric scale parameter $\epsilon = h/H = 1/N$, as well as the effects of microstructural imperfections on these failure surfaces. The imperfections considered are the same geometric and constitutive perturbations defined in equations (9) – (12) of Part I. For all of the finite models considered, the construction of the failure surfaces requires the consideration of the entire representative volume, as opposed to just the unit cell, as in the case of infinite models. The onset of failure is defined by the loss of positive definiteness of the corresponding stiffness matrix $\mathbf{K}$, evaluated along the principal equilibrium solution corresponding to the macroscopic deformation defined by $\mathbf{F}_0(\lambda)$, that is,

$$\lambda_c = \text{ min root of}\left\{\det\left(\mathbf{K}\left(\lambda\right)\right) = 0\right\}, \tag{17}$$

where

$$\mathbf{K} = \frac{\partial^2 \mathcal{E}}{\partial \mathbf{u} \partial \mathbf{u}}, \tag{18}$$

and where $\mathcal{E}(\mathbf{u})$ is the total strain energy of the representative volume, expressed as a function of the internal degrees of freedom $\mathbf{u}$ (recall that Dirichlet boundary conditions are considered). The onset of failure is due to a bifurcation point on the principal solution (for the case of a perfect structure), or due to a limit point (for the case of an imperfect structure).

3 RESULTS

For all of the numerical calculations reported here, the same material parameters that were proposed in Part I for the base element of the unit cell, have been used. The equilibrium solutions for both the unit cell, and for the finite representative volume specimens are determined using an incremental Newton-Raphson algorithm. The critical load parameter surface $\lambda_m(\boldsymbol{\omega})$, determined for the infinite model with perfectly periodic microstructure, and the critical load λ_c, determined for the finite sized specimens, are found using a straightforward bisection method. The results pertaining to the the micro- and macro-failure surfaces for the infinite model are presented and discussed first, followed by the corresponding failure surfaces for finite specimens with both perfectly periodic and imperfect microstructures.

3.1 FAILURE SURFACES FOR THE INFINITE MODEL

Of interest here is the comparison between the micro- and macro-failure surfaces for the perfectly periodic model of infinite extent (to avoid the influence of the model boundaries), as well as the dependence of these failure surfaces on the imposed macroscopic strain. As an illustration, the micro-failure (first bifurcation) and macro-failure (maximum load) points for an infinite lattice model with perfectly periodic microstructure, subjected to uniaxial extension ($\theta = \phi = 0$), are shown along the principal equilibrium path in Figure 1. The corresponding failure surfaces can be constructed using the loci of failure points for all load paths with the same fixed value of the orientation angle θ.

The micro- and macro-failure surfaces for the perfectly periodic, infinite model, are depicted in principal macroscopic strain space in Figure 2 with solid and dashed lines, respectively (recall that λ_1 and λ_2 are the principal stretch ratios which correspond to the macroscopic deformation defined by $\mathbf{F}_0(\lambda)$). The results in Figure 2a correspond to a macroscopic deformation with principal macroscopic strain axes aligned with the initial axes of material orthotropy ($\theta = 0$), while the results in Figure 2b correspond to a macroscopic deformation with principal macroscopic strain axes oriented at an angle $\theta = \pi/8$ with respect to the axes of orthotropy. Note the locations of the first bifurcation and maximum load points, labeled a and b in the uniaxial extension case shown in Figure 1, on the corresponding failure surfaces shown in Figure 2a. Also notice from Figure 2a, that for $\theta = 0$, the macro-failure surface considerably overestimates the critical strains for certain loading directions (approximately for $-\pi/4 \leq \phi \leq \pi/8$ and $3\pi/8 \leq \phi \leq 3\pi/4$).

The stable domain of deformation (i.e. the set of points contained within the micro-failure surface), increases as the principal axes of macroscopic strain rotate with respect to the initial axes of material orthotropy, while the discrepancy between the micro- and macro-failure surfaces decreases significantly,

as one can see for the case when $\theta = \pi/8$ shown in Figure 2b. The strong dependence of the shape of the failure surfaces on the orientation angle θ is one important result of this investigation. Another important result pertains to the fact that these failure surfaces are always closed, and always contain the origin $\lambda_1 = \lambda_2 = 1$. This implies that if the periodic lattice model is adequately strained, it will always lose stability, for any load path starting from the undeformed, stress-free configuration. The fact that the model becomes unstable upon finite straining is a result of the constitutive law chosen to represent the element behavior, which always reaches a maximum load at some finite level of strain. Not all failure surfaces for finitely strained periodic media are closed, as one can see by the example given in Triantafyllidis and Bardenhagen (1997) for a fiber reinforced composite material.

Recall from the discussion in Section 2.1 that the calculations involved in the construction of the micro-failure surface require the determination of the critical load parameter λ_c for each load path, which in turn requires the determination of the critical load parameter surface $\lambda_m(\boldsymbol{\omega})$. Two typical critical load parameter surfaces are depicted in Figure 3, with Figure 3a corresponding to point c on the micro-failure surface shown in Figure 2a, and with Figure 3b corresponding to point d on the same surface. The micro- and macro-failure surfaces do not coincide at point c, thus, the critical load λ_c, which corresponds to the minimum value of $\lambda_m(\boldsymbol{\omega})$ over all dimensionless wave number vectors $\boldsymbol{\omega}$, occurs for $\omega_1 = \omega_2 = \pi$; while at point d, where the micro- and macro-failure surfaces coincide, the minimum occurs at the origin of the dimensionless wave number domain (i.e., at $\omega_1 \to 0$ and $\omega_2 = 0$).

The results for the last portion of the investigation involving the infinite lattice model, pertain to the type of instability mode encountered (e.g., local or global), and verify the validity of the sufficiency condition for the micro- and macro-failure surface separation, based on the parameter β introduced in Section 2.2. The micro-failure surfaces shown in Figure 4 correspond to the same macroscopic straining of the model along the initial axes of material orthotropy ($\theta = 0$), as was considered for the failure surfaces presented in Figure 2a. More specifically, the micro-failure surface depicted in Figure 2a is reploted in Figure 4a, with a solid line representing those critical points for which the instability mode is global in nature (i.e., for which $\omega_c \to 0$), and with a dotted line representing those critical points for which the instability mode is local in nature (i.e., for which $\omega_c \neq 0$). Notice that for the lattice model considered here, the critical mode shape scale parameter is equal to the same value ($\omega_c = \sqrt{2}\pi$) for all critical points for which the micro- and macro-failure surfaces do no coincide. The corresponding bifurcation eigenmodes are always anti-periodic in both coordinate directions, with $\lambda_c = \lambda_m(\pi, \pi)$.

Given the computational advantages associated with determining the macro-failure surface, and the importance of determining the points for which the first instability is accurately predicted by that failure criterion, the failure surface separation parameter β, introduced in equation (15), has been calculated

and plotted in Figure 4b for all critical points on the macro-failure surface previously shown in Figure 2a. The dashed portion of this surface corresponds to those critical points for which $\beta < 0$, while the solid portion corresponds to those critical points for which $\beta \geq 0$. As expected from the discussion of the sufficiency condition, which ensures the onset of a local instability mode when $\beta < 0$, the range of load paths for which $\beta < 0$, is a proper subset of the range for which the micro- and macro-failure surfaces do not coincide.

3.2 FAILURE SURFACES FOR THE FINITE MODELS

a) Perfectly Periodic Model — Influence of Scale

The influence of the relative size of the representative volume, which is characterized by the geometric scale parameter ϵ, on the failure surface of the lattice model with perfectly periodic microstructure, is investigated next for finite sized specimens, subjected to pure biaxial deformations ($\theta = 0$). The results of the corresponding calculations are plotted in Figure 5, with a dotted line representing the failure surface of a coarse 5×5 unit cell model ($\epsilon = 0.2$), with a dashed line representing the failure surface of a more refined 10×10 unit cell model ($\epsilon = 0.1$), and with a solid line representing the failure surface of the corresponding infinite model (i.e., for $\epsilon \to 0$). The latter surface coincides, by definition, with the micro-failure surface shown in Figure 2a. As expected, the failure surfaces of the finite sized models converge monotonically to the failure surface of the infinite model, as the geometric scale parameter ϵ converges to zero (due to the progressive reduction in the stiffening influence of the prescribed displacement boundary conditions). Moreover, the influence of the geometric scale parameter ϵ on the failure surface is negligible only in a small subset of the range of deformations for which the micro- and macro-failure surfaces for the infinite model coincide, namely, for the range near the balanced biaxial extension load path (compare the coincident regions of the failure surfaces in Figure 5 with the appropriate portion of the micro-failure surface shown in Figure 4a, for which $\omega_c \to 0$).

Additional information about the nature of the eigenmode at the onset of failure (i.e., whether the instability mode is local or global in nature), for the finite model with perfectly periodic microstructure, can be obtained from information about the critical mode shape scale parameter ω_c, for the corresponding infinite model shown Figure 4a. The eigenmodes shown in Figures 6a and 6b are for a finite lattice model with $\epsilon = 0.1$, and correspond to the failure points labeled c and d on the failure surface of the infinite model shown in Figure 2a (i.e., for load paths with $\phi = 25°$ and $\phi = 35°$, respectively). As expected from the corresponding critical load parameter surfaces shown in Figure 3a and Figure 3b, the shape of the eigenmode for the local instability corresponding to point c, is anti-periodic (with a wavelength equal to

two unit cell lengths in each direction) near the center of the model (i.e., away from the boundaries), as shown in Figure 6a; while the shape of the eigenmode for the global instability corresponding to point d, varies smoothly over the entire specimen, as shown in Figure 6b.

b) Imperfect Models — Influence of Imperfections

The final part of this investigation addresses the influence of microstructural imperfections on the failure surfaces of finite lattice models. The imperfections considered are either geometric or constitutive in nature, and are described by equations (9) – (12) of Part I. With regard to the failure surfaces of the finite model with perfectly periodic microstructure, the results presented here correspond to pure biaxial deformations along the initial axes of material orthotropy ($\theta = 0$). In addition, all of the calculations correspond to a 25×25 unit cell model ($\epsilon = 0.04$), since for this, or any smaller values of the geometric scale parameter ϵ, there is no appreciable influence on the corresponding failure surfaces (for $\epsilon = 0.04$ the failure surface of the finite model with perfectly periodic microstructure nearly coincides with the failure surface of the infinite model).

As expected from general imperfection sensitivity theory for the buckling of elastic structures (see, for example, Budiansky, 1974), the maximum load for the lattice model with microstructural imperfections is lower than the load corresponding to the initial bifurcation point for the perfectly periodic counterpart. This phenomenon occurs when the post-bifurcation equilibrium solution of a perfect structure is subcritical (i.e., when the solution occurs under a decreasing applied load). For lattice structures with individual elements which exhibit a maximum load (as in the present case), one can show that the corresponding bifurcated equilibrium solutions are subcritical under either load or displacement control, since they emerge under decreasing load and decreasing displacement (see Triantafyllidis and Bardenhagen, 1993). Consequently, the imperfect structure exhibits a critical load along any load path through strain space. Moreover, the general theory of elastic stability dictates that the maximum load of the imperfect structure decreases with increasing amplitude of imperfection. Hence, the failure surfaces for the imperfect, finite lattice models, with a given imperfection shape, are contained within (i.e., bounded from above by) the failure surface for the corresponding perfectly periodic model. Furthermore, the failure surfaces for the imperfect models contract monotonically with increasing imperfection amplitude parameter δ.

The influence of the imperfection amplitude parameter δ on the failure surface of the perfectly periodic, finite model is shown in Figure 7a and Figure 7b for regular ($m_1 = m_2 = 2$) geometric and constitutive imperfections, respectively. The choice of imperfection shape is motivated by the desire to leave the initial average stiffness of the model unchanged. The results correspond to two different values of the imperfection amplitude parameter: $\delta = 0.1$ and $\delta = 0.25$, represented by dashed and dotted lines,

respectively. The maximum discrepancy between the critical load parameter λ_c, determined for the perfectly periodic and imperfect models, occurs for both geometric and constitutive imperfections, for a deformation corresponding to pure balanced biaxial extension ($\phi = \pi/4$). The maximum reduction in the critical load due to geometric imperfections is approximately 8.5% for an imperfection amplitude corresponding to $\delta = 0.1$, and is approximately 17% for $\delta = 0.25$, as seen in Figure 7a. The corresponding reductions due to constitutive imperfections are approximately 19% and 36%, respectively. The main conclusion drawn from this portion of the investigation is that for an adequately large, but fixed amplitude of imperfection, the regular constitutive imperfections have a stronger influence on the micro-failure surfaces than their geometric counterparts.

For a fixed imperfection amplitude parameter (for the calculations considered here $\delta = 0.25$) the influence of the imperfection shape on the failure surface of the finite models, subjected to pure biaxial deformations ($\theta = 0$) is shown in Figure 8a for the case of geometric imperfections, and in Figure 8b for the case of constitutive imperfections. For the case of geometric imperfections, the maximum load decreases with increasing imperfection wave number (i.e., with decreasing imperfection wavelength) and hence, the corresponding failure surfaces are contained within (i.e., bounded from above by) the failure surface of the perfectly periodic model, accordingly. The most contracted failure surface corresponds to a geometric imperfection with a random shape, and shows a significant reduction in the critical load (up to 50%, compared with 17% for the case of a model with regular $m_1 = m_2 = 2$ geometric imperfections, subjected to balanced biaxial extension), as seen in Figure 8a.

In contrast to the strong influence of the geometric imperfection shape on the failure surface of the finite model, the influence of the constitutive imperfection shape is less pronounced (the maximum reduction in the critical load is on the order of 36%), as seen in Figure 8b. Also, in contrast to the results presented in Figure 8a, the critical loads for the models with constitutive imperfections do not decrease monotonically with the wavelength of the regular imperfection shape (notice that the failure surface for the model with random constitutive imperfections is nested between the failure surfaces for the models with regular imperfections). One should also notice at this point, that unlike the results presented in Figure 7 for models with regular imperfections, where for a fixed imperfection amplitude parameter δ, the constitutive imperfections resulted in a more contracted failure surface, the opposite is true for models with random imperfections (i.e., for a given imperfection amplitude, a random geometric imperfection weakens the model more than a random constitutive imperfection).

4 CONCLUSIONS

In the second part of this work, attention is focused on the influence of scale on the stability of microstructured media. Using the same nonlinearly elastic lattice model introduced in Part I, failure is defined as the onset of the first instability encountered along a radial load path through macroscopic strain space. Failure surfaces are then constructed using the locus of failure points for all load paths corresponding to a fixed value of the principal macroscopic strain orientation angle. Subsequently, the influence of the geometric scale and microstructural imperfection parameters on the failure surfaces of the model are investigated.

For the case of an infinite lattice model with perfectly periodic microstructure, the relevant scale is characterized by the mode shape scale parameter ω, which is defined as the ratio of the unit cell size, to the wavelength of the first instability mode. Using Bloch wave theory on the deformed configuration of the unit cell, the "*micro-failure*" surface for the model is constructed in macroscopic strain space. In addition, the critical value of the mode shape scale parameter ω_c is determined for each point on the micro-failure surface. The critical points for which $\omega_c \neq 0$ correspond to local first instability modes, while the points for which $\omega_c = 0$ correspond to first instability modes which are global in nature.

For the infinite model with perfectly periodic microstructure, the concept of a "*macro-failure*" surface is also introduced. This surface is defined as the locus of all points in macroscopic strain space for which the macroscopic (homogenized) response of the model loses ellipticity. The corresponding calculations are based on the determination of the overall properties of the unit cell at a given state of deformation, and are considerably less intensive computationally than the Bloch wave calculations involved in the determination of the corresponding micro-failure surface. It can be shown that the two failure surfaces coincide when the critical mode shape scale parameter ω_c approaches zero. Consequently, the micro-failure surface is always contained within (i.e., bounded from above by) the more easily obtainable macro-failure surface. The range of deformations for which the two surfaces coincide (i.e., the range for which $\omega_c \to 0$) is the range of deformations which are expected to result in post-failure behavior of the model involving a catastrophic macroscopic localization of deformation.

For the case of finite sized specimens, the failure surface is also a function of the geometric scale parameter ϵ (i.e., the ratio of the size of unit cell, to the size of representative volume). Due to the stiffening influence of the imposed Dirichlet boundary conditions, the failure surfaces for the perfectly periodic, finite models are bounded from below by the micro-failure surface of the infinite model, and converge monotonically to the infinite model failure surface, as the geometric scale parameter approaches zero. For specimen sizes with $\epsilon < 0.04$ ($N > 25$) the geometric scale effects become negligible.

Of particular importance is the influence of microstructural imperfections on the failure surfaces of the finite models. For a regular (smoothly varying) imperfection shape with a fixed wavelength, the failure surfaces for the imperfect models are bounded from above by the failure surface of the corresponding perfectly periodic model, and contract monotonically with increasing imperfection amplitude. For finite models with geometric imperfections of fixed amplitude, the failure surfaces also contract monotonically with increasing wave number (i.e., with decreasing wavelength), with the most contracted surface corresponding to the random imperfection shape. This result does not hold for the case of models with constitutive imperfections.

The proposed methodology of introducing a failure surface to study the effects of scale on the failure of ductile media with periodic or nearly periodic microstructures is general. Furthermore, the failure surfaces introduced here can be defined in either macroscopic strain or macroscopic stress space. The relatively simple lattice model, which admits computationally efficient solutions, provides considerable insight into the stability problems of more complicated microstructured media. The extreme sensitivity of the shape of the failure surfaces to the macroscopic load orientation has been established. Moreover, the failure surface calculations give the critical mode shape scale (e.g., local or global) at the onset of failure. What is more important, is that the failure surface for the infinite model with perfectly periodic microstructure, determined using Bloch wave theory, provides an upper bound for the failure surfaces of the more realistic, imperfect models.

The sequence of calculations proposed to establish the failure surfaces for the perfectly periodic medium proceed from the simplest (construction of the macro-failure surface for the perfectly periodic, infinite model), to the more complex (construction of the micro-failure surface), and illustrate how to bound the actual failure surface of a real (imperfect) microstructured medium, for which the failure calculations in an actual application would be prohibitively time consuming. The ideas developed are intended for applications to more realistic microstructured materials, i.e. composites with more complicated microgeometries (e.g. honeycombs, foams, fiber reinforced composites) and constitutive equations (e.g. rate–independent elastoplastic). Work in that direction has already been initiated, starting with applications involving aluminum honeycombs (Triantafyllidis and Schraad, 1997), and fiber-reinforced composites (Triantafyllidis and Bardenhagen, 1996). Calculations of the onset of failure surfaces in these applications require only the current tangent moduli, just as in the nonlinear elastic material case. The unloading feature of plasticity becomes important only in the postbuckling and localization part of the response, thus justifying the nonlinear elasticity simplifiaction adopted in the present work.

ACKNOWLEDGMENTS

The present work was partially funded, initially by Alcoa, and subsequently by AFOSR under Grant DOD-G-F49620-94-1-0402. The authors would like to express their appreciation for this financial assistance, and their gratitude to Dr. Owen Richmond of the Alcoa Technical Center for his interest and encouragement, and for sharing his ideas on the subject of stability as it relates to microstructured materials.

References

[1] Anderson, M. S. (1981) Buckling of periodic lattice structures. *AIAA J.* **19**, 782-788.

[2] Anderson, M. S. (1986) Natural vibration and buckling of general periodic lattice structures. *AIAA J.* **24**, 163-169.

[3] Budiansky, B. (1974) Theory of buckling and post-buckling behavior of elastic structures. In *Advances in Applied Mechanics* (Edited by C. H. Yih), 1-65. Academic Press, New York.

[4] Elyada, D. and Babcock, C. (1987) Buckling and nonlinear response of imperfect three-legged truss columns. *AIAA J.* **25**, 324-330.

[5] Forman, S. and Hutchinson, J. W. (1970) Buckling of reticulated shell structures. *Int. J. Solids Structures* **6**, 909-932.

[6] Geymonet, G., Müller, S. and Triantafyllidis, N. (1993) Homogenization of nonlinearly elastic materials, microscopic bifurcation and macroscopic loss of rank-one convexity. *Arch. Rat. Mech. Anal.* **122**, 231-290.

[7] Greszczuk, L. B. (1975) Microbuckling failure in circular fiber-reinforced composites. *AIAA J.* **13**, 1311-1318.

[8] Lomont, J. S. (1959) *Applications of finite groups.* Academic Press, New York.

[9] Triantafyllidis, N. and Bardenhagen, S. (1993) On higher order gradient continuum theories in 1-D nonlinear elasticity. Derivation from and comparison to the corresponding discrete models. *J. Elasticity* **33**, 259-293.

[10] Triantafyllidis, N. and Bardenhagen, S. (1996) The influence of scale size on the stability of periodic solids and the role of associated higher order gradient continuum models. *J. Mech. Phys. Solids* **44**, 1891-1928.

[11] Triantafyllidis, N. and Maker, B. N. (1985) On the comparison between microscopic and macroscopic instability mechanisms in a class of fiber-reinforced composites. *J. Appl. Mech.* **52**, 794-800.

[12] Triantafyllidis, N. and Schnaidt, W. C. (1993) Comparison of microscopic and macroscopic instabilities in a class of two-dimensional periodic composites. *J. Mech. Phys. Solids* **41**, 1533-1565.

[13] Triantafyllidis, N. and Schraad, M. (1997) Onset of failure in aluminum honeycombs under general in-plane loading. *J. Mech. Phys. Solids* submitted.

FIGURE CAPTIONS

Figure 1: Micro- and macro-failure points, corresponding to the initial bifurcation in the principal equilibrium solution and the loss of ellipticity in the macroscopic material behavior, respectively, for an infinite lattice model ($\epsilon \to 0$) with perfectly periodic microstructure ($\delta = 0$), subjected to uniaxial extension with no lateral contraction ($\phi = \theta = 0$).

Figure 2: Micro- and macro-failure surfaces, corresponding to the initial bifurcation in the principal equilibrium solution and the loss of ellipticity in the macroscopic material behavior, respectively, in macroscopic strain space, for an infinite lattice model ($\epsilon \to 0$) with perfectly periodic microstructure ($\delta = 0$), subjected to (a) pure biaxial deformations ($\theta = 0$) and (b) deformations including shear ($\theta = \pi/8$).

Figure 3: Critical load parameter surface, determined using Bloch wave theory, for an infinite lattice model ($\epsilon \to 0$) with perfectly periodic microstructure ($\delta = 0$), subjected to (a) pure biaxial extension with $\phi = 25^\circ$ and (b) pure biaxial extension with $\phi = 35^\circ$.

Figure 4: (a) Values of the critical bifurcation mode shape scale parameter ω_c, for an infinite lattice model ($\epsilon \to 0$) with perfectly periodic microstructure ($\delta = 0$), subjected to pure biaxial deformations ($\theta = 0$). (b) Corresponding values of the failure criterion β based on the higher order macroscopic (homogenized) moduli.

Figure 5: Scale effects on the micro-failure surfaces of perfectly periodic lattice models ($\delta = 0$), subjected to pure biaxial deformations ($\theta = 0$). Note that the micro-failure surface, determined using Bloch wave theory for the infinite model, provides a lower bound for the failure surfaces of the finite models.

Figure 6: Bifurcation mode shapes for a finite lattice model ($\epsilon = 0.1$) with perfectly periodic microstructure ($\delta = 0$), subjected to (a) pure biaxial extension with $\phi = 25^\circ$ and (b) pure biaxial extension with $\phi = 35^\circ$.

Figure 7: Sensitivity of the micro-failure surface to the magnitude of the imperfection amplitude parameter δ, for finite lattice models ($\epsilon = 0.04$) with regular ($m_1 = m_2 = 2$) (a) geometric imperfections and (b) constitutive imperfections, subjected to pure biaxial deformations ($\theta = 0$). Note that the micro-failure surface determined for the perfectly periodic model, provides an upper bound for the failure surfaces of the imperfect models.

Figure 8: Sensitivity of the micro-failure surface to the imperfection shape for finite lattice models ($\epsilon = 0.04$) with (a) geometric imperfections and (b) constitutive imperfections of twenty-five percent amplitude ($\delta = 0.25$), subjected to pure biaxial deformations ($\theta = 0$).

FIGURES

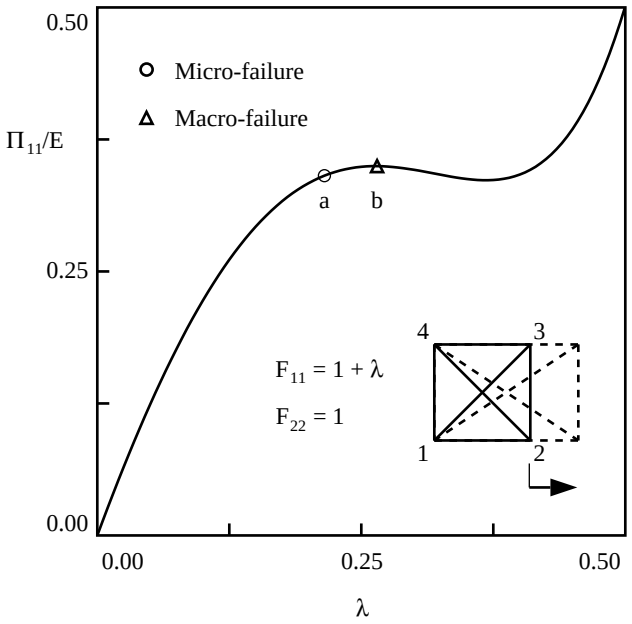

Figure 1: See FIGURE CAPTIONS

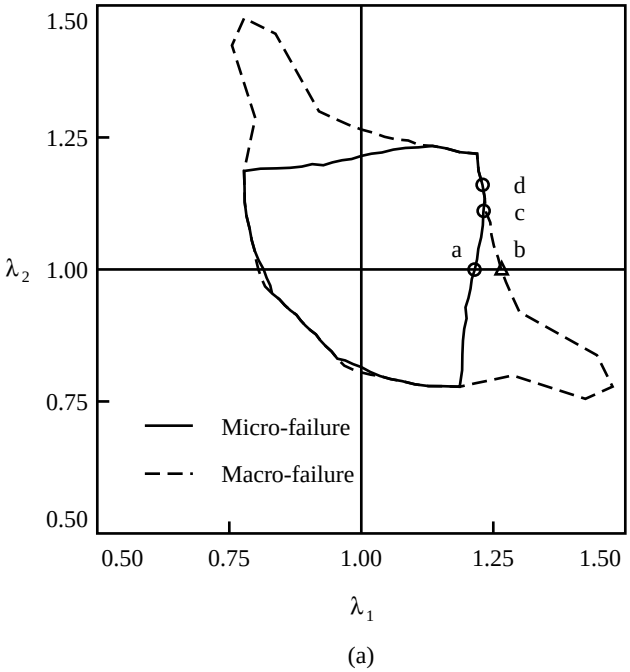

(a)

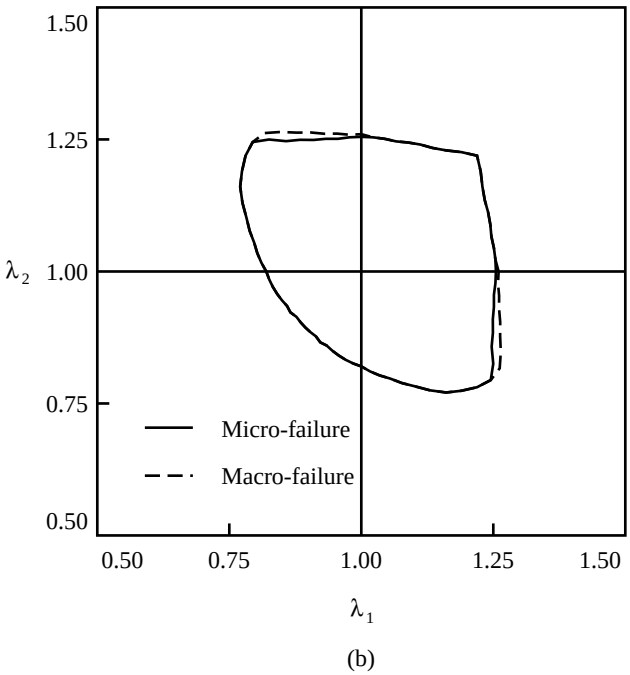

(b)

Figure 2: See FIGURE CAPTIONS

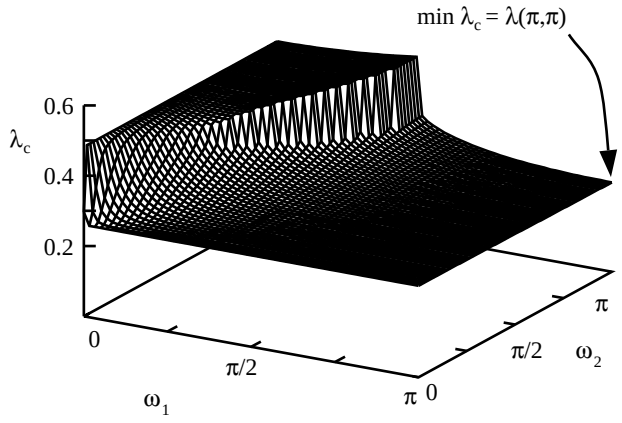

(a)

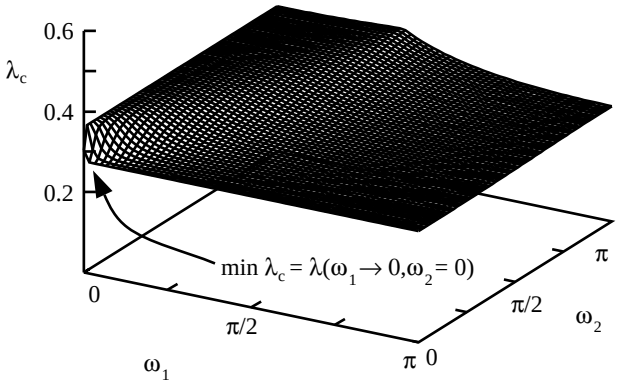

(b)

Figure 3: See FIGURE CAPTIONS

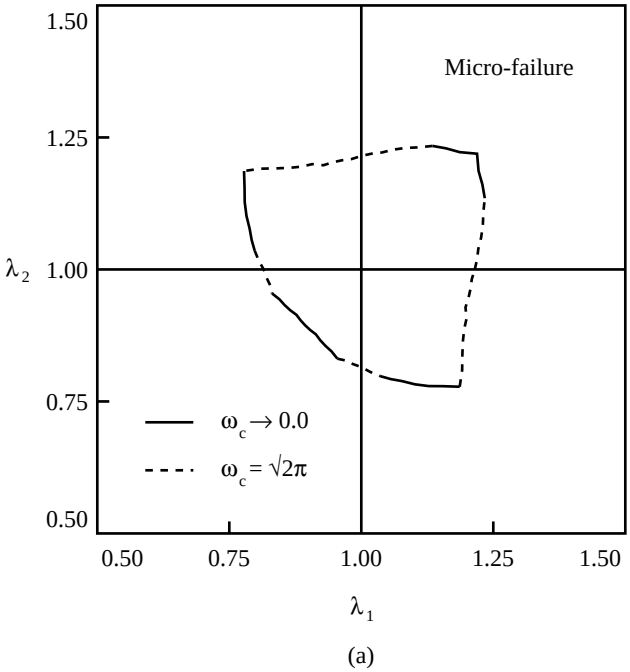

(a)

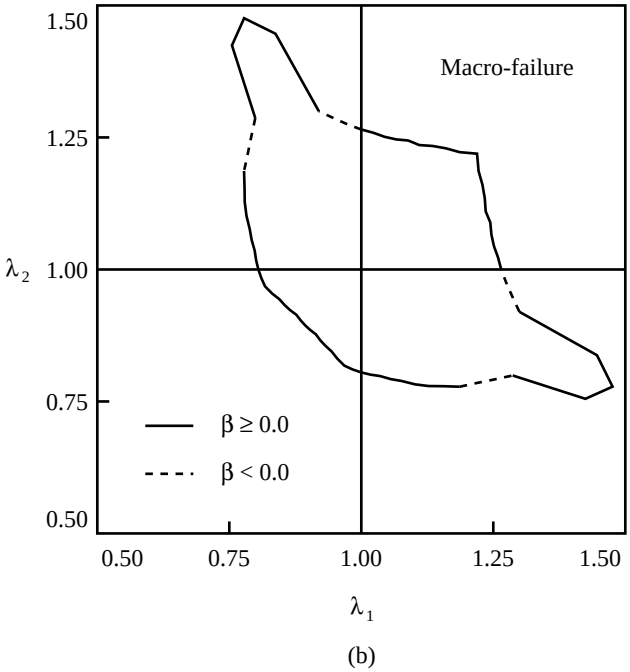

(b)

Figure 4: See FIGURE CAPTIONS

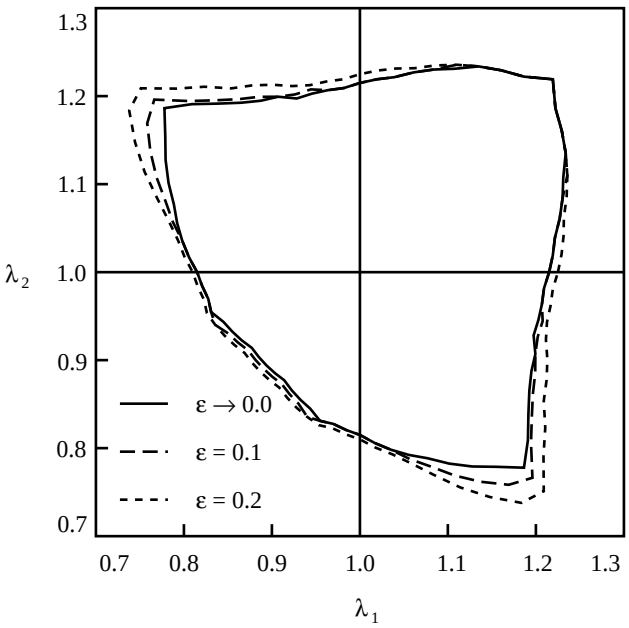

Figure 5: See FIGURE CAPTIONS

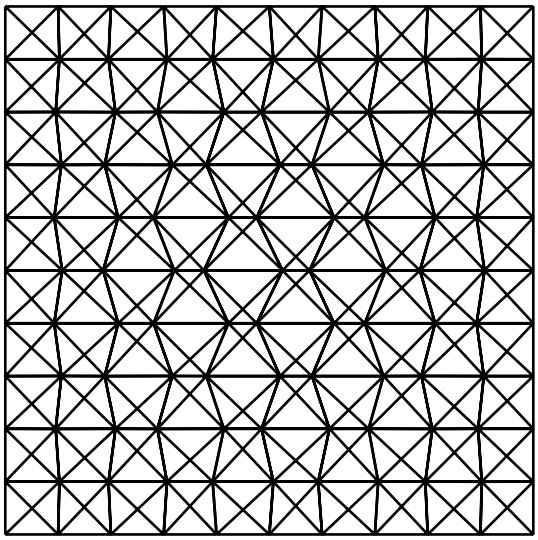

(a)

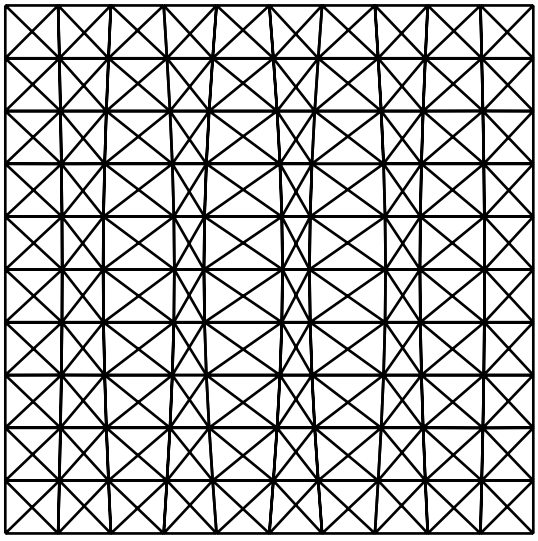

(b)

Figure 6: See FIGURE CAPTIONS

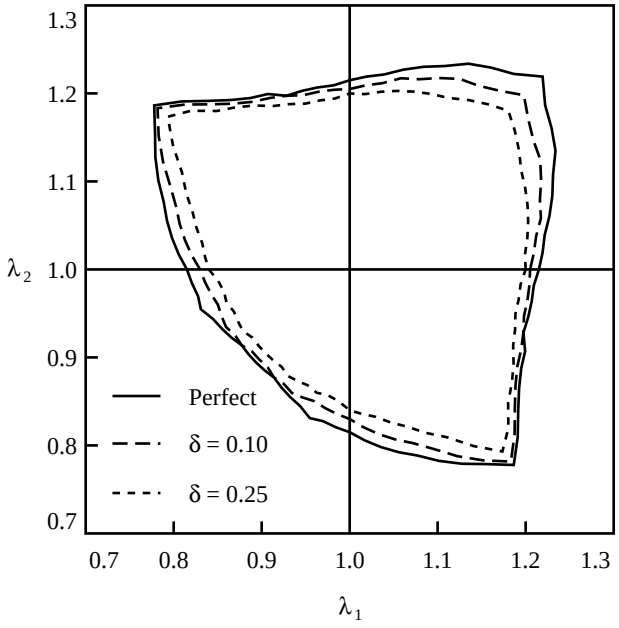

(a)

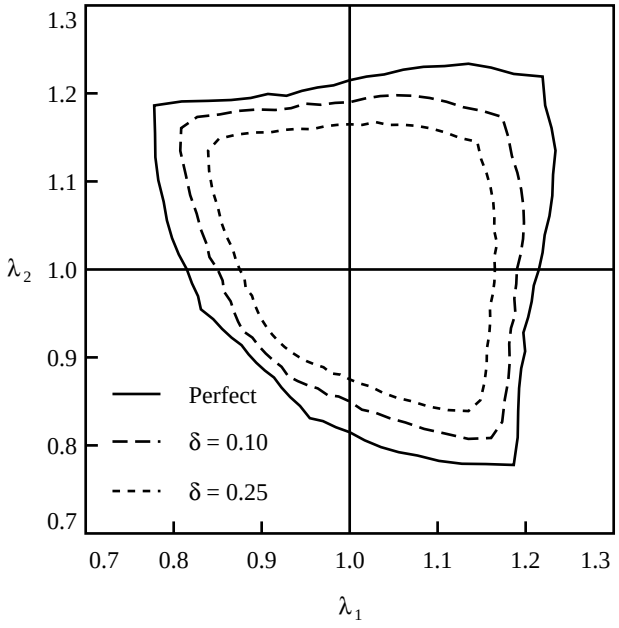

(b)

Figure 7: See FIGURE CAPTIONS

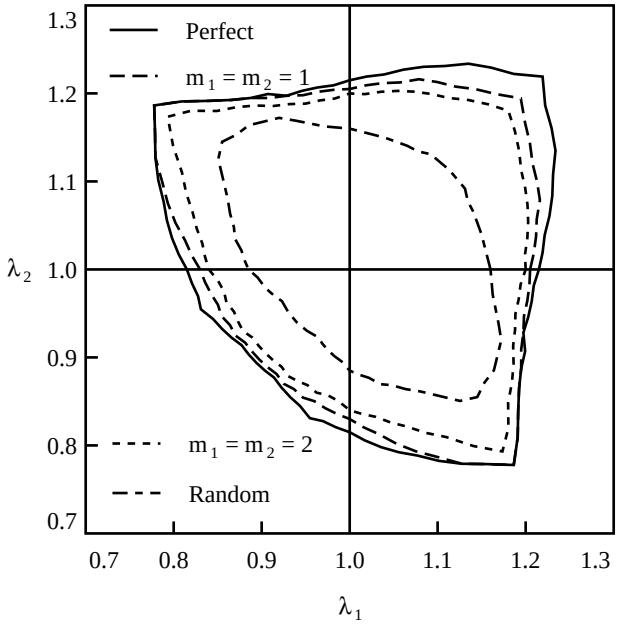

(a)

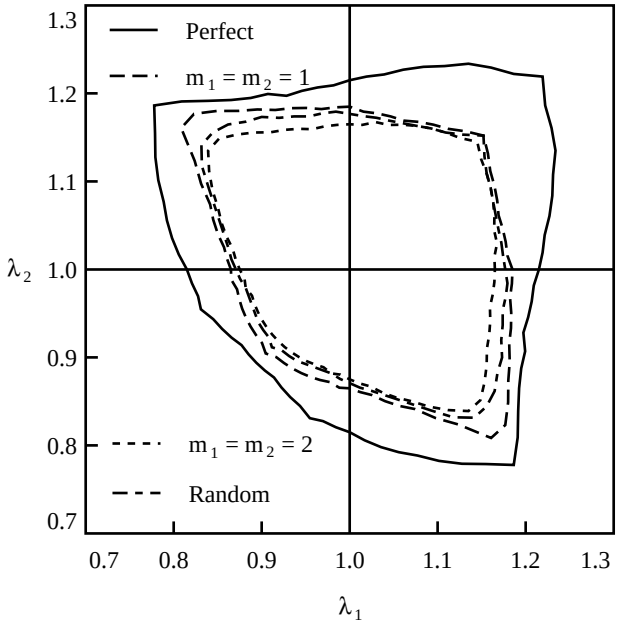

(b)

Figure 8: See FIGURE CAPTIONS